ACS APPLIED MATERIALS & INTERFACES

Research Article

Cite This: ACS Appl. Mater. Interfaces 2020, 12, 1465−1473

www.acsami.org

High-Speed All-Optical Modulator Based on a Polymer Nanofiber Bragg Grating Printed by Femtosecond Laser

Changrui Liao,*[,†,‡,⊥] Chi Li,[†,‡,⊥] Chao Wang,[§] Ying Wang,[†,‡] Jun He,[†,‡] Shen Liu,[†,‡] Zhiyong Bai,[†,‡] Zongsong Gan,[∥] and Yiping Wang[†,‡]

[†]Guangdong and Hong Kong Joint Research Centre for Optical Fibre Sensors, Shenzhen University, Shenzhen 518060, China

[‡]Key Laboratory of Optoelectronic Devices and Systems of Ministry of Education and Guangdong Province, College of Physics and Optoelectronic Engineering, Shenzhen University, Shenzhen 518060, China

[§]Department of Electrical Engineering and Photonics Research Center, The Hong Kong Polytechnic University, Hung Hom, Kowloon, Hong Kong, China

[∥]Wuhan National Laboratory for Optoelectronics (WNLO), Huazhong University of Science and Technology (HUST), Wuhan 430074, China

Supporting Information

ABSTRACT: On-chip optical modulator for high-speed information processing system has been widely investigated by many researchers, but the connection with the fiber system is difficult. The fiber-based optical modulator is a good solution to this problem. Fiber Bragg Grating has good potential to be used as an optical modulator because of its linear temperature response, narrow bandwidth, and compact structure. In this paper, a new fiber-integrated all-optical modulator has been realized based on a polymer nanofiber Bragg grating printed by a femtosecond laser. This device exhibits a fast temporal response of 176 ns and a good linear modulation of −45.43 pm/mW. Moreover, its stability has also been studied. This work first employs Bragg resonance to realize a fiber-integrated all-optical modulator and paves the way toward realization of multifunctional lab-in-fiber devices.

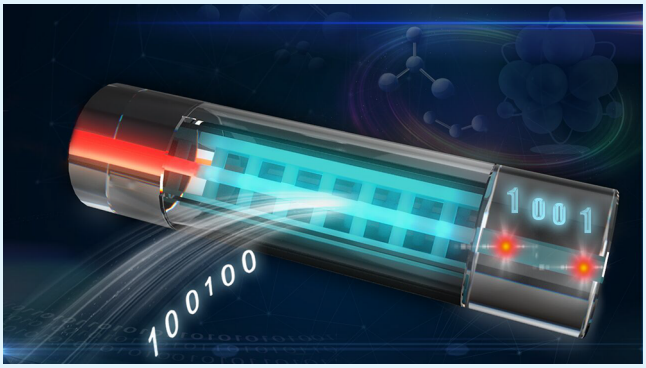

KEYWORDS: *all-optical modulator, polymer fiber, fiber Bragg grating, multiphoton polymerization, femtosecond laser micromachining*

1. INTRODUCTION

Optical modulators are playing increasingly significant roles in modern information processing technology. To date, various methods have been presented to achieve on-chip optical modulators with fast and low-energy-consumption. For example, Xu et al. reported a silicon electro-optic modulator with a footprint of a few micrometers based on a light-confining resonant structure.[1] Xie et al. demonstrated an on-chip dual electro-optic and opto-electric modulator based on a composite microstructure with a 2D silicon nitride (SiN) photonic crystal slot waveguide and a photonic crystal nanocavity covered by a zinc oxide (ZnO) nanowire.[2] Comparing with the on-chip optical modulators, the fiber-integrated optical modulators have more advantages in connecting with optical fiber systems.[3−5] Utilizing the electrical properties of 2D materials is a typical approach to realize fiber-integrated modulator. Yu et al. employed graphene to develop an interferential all-optical fiber switch and achieved a fast temporal response of ∼3 ns.[6] Mao et al. employed ReS_2 to implement passively Q-switched and mode-locked fiber lasers.[7] However, this method usually exhibits weak structural stability, high power trigger threshold, and nonlinear modulation response. Szukalski et al. demonstrated an intriguing all-optical switch based on deoxyribonucleic acid (DNA) in the form of electrospun fibers, and its temporal response was ∼0.35 ms.[8] A practical fiber-integrated optical modulator needs both good structural stability and a relatively low power trigger threshold.

Fiber Bragg grating (FBG) is a good candidate for fiber-integrated optical modulator because of its linear thermal response, very narrow bandwidth, and compact size.[9,10] Liao et al. reported that the temporal thermal response of the silica FBG is ∼1 ms, being limited by the low thermo-optical coefficient (∼6.45 × 10^{-6}/°C) of silica, and the power trigger threshold is also very high.[11] Therefore, it is not possible for silica FBG to be used as an optical modulator. Recently, polymers have been widely used in optofluidic devices, microelectromechanical systems (MEMS), and metamaterials[12−14] for cell detection, photomechanical research, and

Received: September 20, 2019
Accepted: December 9, 2019
Published: December 9, 2019

DOI: 10.1021/acsami.9b16716
ACS Appl. Mater. Interfaces 2020, 12, 1465−1473

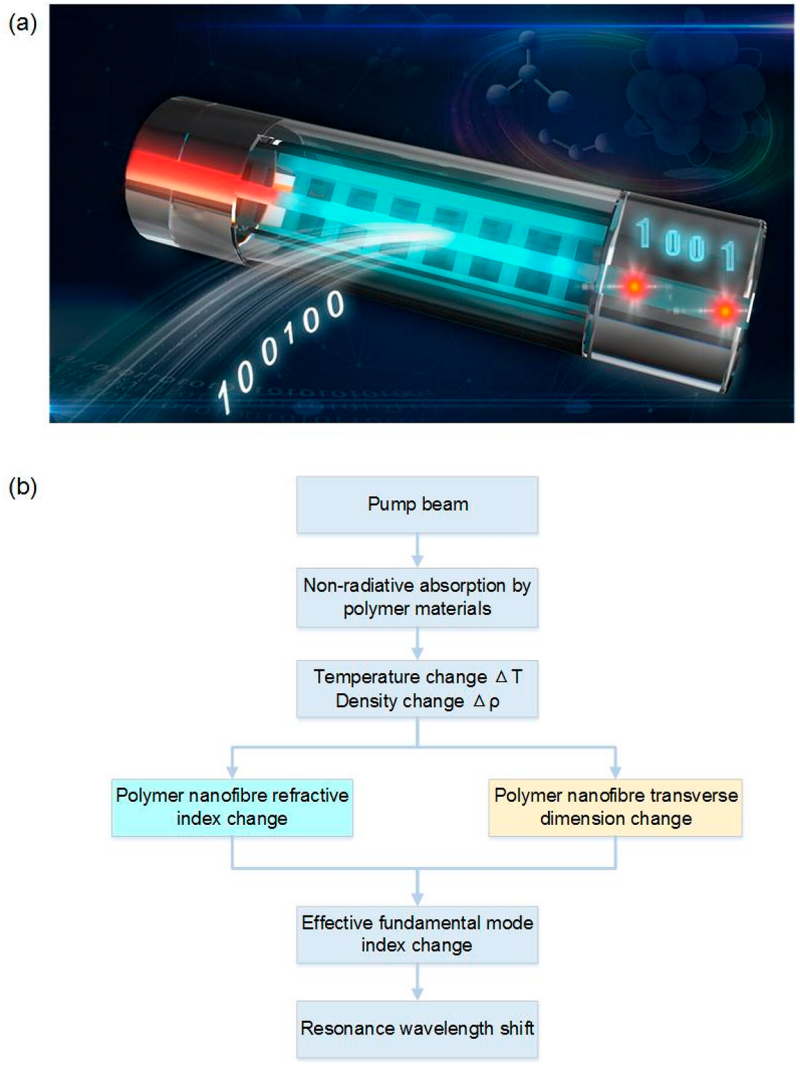

Figure 1. (a) Schematic diagram of the all-optical modulator based on a polymer NFBG. The probe light is in red and the pump light (100100) is in white. (b) Processes involved in producing the Bragg resonant wavelength shift of the polymer NFBG.

environmental monitoring because of their high thermal-optical coefficient ($\sim -2 \times 10^{-4}/°C$), simple surface modification, and good plasticity.[15] Moreover, some polymer structures in the nanoscale exhibited fast temporal thermal response based on a photothermal (PT) effect.[16−18] Inspired by these efforts, we proposed a polymer nanofiber Bragg grating (NFBG) configuration being integrated in a silica hollow fiber aiming to realize a high-speed fiber-integrated optical modulator with a linear response and a low power trigger threshold.

In this work, the fiber device was fabricated by use of femtosecond (Fs) laser subtractive manufacturing (ablation) and additive manufacturing (multiphoton polymerization, MPP). The polymer structure was completely embedded in a section of hollow core fiber (HCF), realizing a highly integrated fiber device. Static and dynamic optical pump responses have been experimentally investigated, and a pump sensitivity of −45.43 pm/mW and a temporal response of ∼176 ns were obtained, which were much better than the silica FBG modulator and traditional polymer devices.[19,20] Compared with 2D material based modulators, our device has a linear response, lower power trigger threshold, and better mechanical stability. The power range of normal operation and the humidity influence have also been experimentally investigated. This method also has potential to realize some functional tunable lenses for the biosensing or chemical sensing fields.[21,22]

2. WORKING PRINCIPLE

The working principle of this modulator is demonstrated in Figure 1(a). The polymer structure printed by Fs laser MPP was embedded in a silica HCF being spliced between two thin-core fibers (TCFs). A pair of polymer bases are designed to reinforce the whole polymer structure, and the grating segments are designed to lift the central polymer nanofiber and excite Bragg resonance in it. To begin with, the probe light (red color) and the pump light (white color) are simultaneously coupled into the polymer NFBG by use of a WDM coupler. The Bragg resonant wavelength of the NFBG will experience a synchronous shift with the excitation of pump light; thus the probe light can be modulated by spectral filtering to realize optical modulation.

The flowchart in Figure 1(b) describes the theoretical basis of PT spectroscopy in the polymer NFBG. When the pump light was coupled into the polymer NFBG, it was absorbed by the polymer material, and the polymer molecular chains were

DOI: 10.1021/acsami.9b16716
ACS Appl. Mater. Interfaces 2020, 12, 1465−1473

excited in a nonradiative manner and then return to the equilibrium state. This process was accompanied by periodic heat production, which can simultaneously modulate the local temperature and the density of the polymer nanofiber (NF) and, as a consequence, the effective refractive index of the NF was modulated.[23] As a result, the resonant wavelength of the polymer NFBG was shifted.

The intensity profile I(r, z) of the pump light can be approximated by a Gaussian distribution:[24]

$$I(r, z) \approx I_0(z)e^{-2r^2/\omega^2} = \frac{2P_{\text{pump}}(z)}{\pi\omega^2}e^{-2r^2/\omega^2} \quad (1)$$

where $I_0(z)$ is the pump light intensity at the center of the fiber core, which decreases with the propagation distance (z) because of nonradiative material absorption and intrinsic attenuation. P_{pump} is the power of pump light, r is the distance from the center of the spherical wave to the observation point, and 2ω is the mode field diameter (MFD), which is same with the diameter of the polymer NF. If the heat yield is Y_H, then the local heat production rate from weak optical absorption can be expressed as[25]

$$H(r, z) = Y_H\theta X1(\lambda_{\text{pump}})I(r, z) \quad (2)$$

where $\overline{X}(\lambda)$ is the peak normalized absorption line-shape function and θ is the peak absorption coefficient of the photoresin used in this work. When the pump light is turned on at $t = 0$, the intensity $I(t)$ through the polymer NFBG is given by[26]

$$\frac{I(t)}{I(0)} = \frac{1}{\left[1 - \frac{\theta}{1+\frac{t_c}{t}} + \frac{\theta^2}{2\left(1+\frac{t_c}{t}\right)^2}\right]} \quad (3)$$

where the relaxation time in the heating process is described as

$$t_c = \frac{\omega_1^2}{4\alpha} \quad (4)$$

where ω_1 is the beam radius irradiated on the NF and α is the thermal diffusivity coefficient of the material. When the thermal diffusivity coefficient of the polymer material is generally about 0.18 mm^2/s[27,28] and the beam radius is about 0.325 μm, which is similar to the radius of the used NF, t_c then can be calculated as 1.47×10^{-7} s (147 ns). The variations of the temperature and the volume of the polymer NFBG can be expressed as

$$\Delta T = k_1\theta\overline{X}(\lambda_{\text{pump}})(I(0) - I(t)) \quad (5)$$

$$\Delta V = k_2\theta\overline{X}(\lambda_{\text{pump}})(I(0) - I(t))\frac{\partial V}{\partial T} \quad (6)$$

where k_1 and k_2 are proportionality coefficients. Due to the material's thermal expansion, the heating process causes the NF volume to increase and its density to decrease. Furthermore, the refractive index of the polymer decreases due to its negative thermo-optical coefficient. The refractive index change can be written as a sum of the different contributions:[29]

$$\Delta n = \left(\frac{\partial n}{\partial \rho}\right)_T\left(\frac{\partial \rho}{\partial T}\right)\Delta T + \left(\frac{\partial n}{\partial T}\right)_\rho \Delta T + \left(\frac{\partial n}{\partial V}\right)_T \Delta V \quad (7)$$

where the first two terms are due to the heat release of the nonradiative decay of the photoinduced transient species, and they express the density and the temperature terms. The third term contains the density due to structural volume changes of the polymer NFBG. According to the Bragg resonance formula, the accumulated resonant wavelength change of the fundamental mode can be expressed as[30]

$$\Delta\lambda_b = k_3 \cdot \Delta n \cdot \Lambda \quad (8)$$

where k_3 is a proportionality coefficient and Λ is the grating pitch. When the wavelength of probe light is matched to the Bragg resonant wavelength, the pump-light-induced grating spectral shift will lead to the power change of probe light, thereby achieving the all-optical modulation.

3. DEVICE FABRICATION

A new photoresist (PR) with good mechanical strength has been developed to print fiber-integrated polymer NFBG. The PR included a photoinitiator (IGR-369, Ciba-Geigy) with a mole ratio of 2.5%, trifunctional monomer SR444 (pentaerythritol triacrylate, Sartomer) with a mole ratio of 40%, trifunctional monomer SR368 (Tris (2-hydroxyethyl) isocyanurate triacrylate, Sartomer) with a mole ratio of 30%, and trifunctional monomer SR454 (ethoxylated3 trimethylolpropane triacrylate, Sartomer) with a mole ratio of 25%. These were mixed and dissolved in acetone. To guarantee sufficient dissolution, the mixture was heated at 50 °C for 1 h. Then, 4-hydroxyanisole (MEHQ, Sigma-Aldrich), as a polymerization inhibitor, was added to the mixture with a mole ratio of 0.5%. After the complete dissolution of the MEHQ, the mixture was heated to 120 °C. Then, tetraethylthiuram disulfide (TED, Sigma-Aldrich) with a mole ratio of 2.0% was used as an accelerator promoter, and the mixture was maintained at 120 °C for 10 min. A centrifuge was used to remove any undissolved chemicals. The mixture was vacuumed to remove residual acetone. The final PR was heated at 60 °C for 1 h. SR368 was used to improve the chemical reactivity for high photosensitivity and mechanical strength against damage and shrinkage during the developing process. SR444 was introduced to prevent the viscosity from decreasing the photoinhibition efficiency. SR454 was used to improve the mechanical strength of PR. TED was used to further improve the mechanical strength. The single-photon absorbance spectrum of the PR is shown in Figure 2.[31]

We proposed an original fabrication method to realize the fiber-integrated polymer micro/nanostructure, which can be divided into four steps, illustrated in Figure 3.[32]

Step 1: In Figure 3(a1), by use of a precise cutting system, a section of HCF with internal/external diameters of 15/120 μm was spliced between two TCFs with core/cladding diameters of 5.8/125 μm. The splicing parameters should be optimized to avoid an air hole collapse at the splicing joint. An optical microscope image of the sandwiched structure (TCF-HCF-TCF) is shown in Figure 3(a2).

Step 2: In Figure 3(b1), a pair of rectangular grooves (each groove was 800 μm × 25 μm × 60 μm) were successively drilled by Fs laser ablation from the upper and lower surfaces of the HCF to open the air hole so that the liquid PR can flow in. The sample was then carefully cleaned with alcohol under ultrasonic conditions for approximately 5 min to remove the residual debris generated during laser ablation. An optical microscope image of the grooved HCF is shown in Figure 3(b2).

DOI: 10.1021/acsami.9b16716
ACS Appl. Mater. Interfaces 2020, 12, 1465−1473

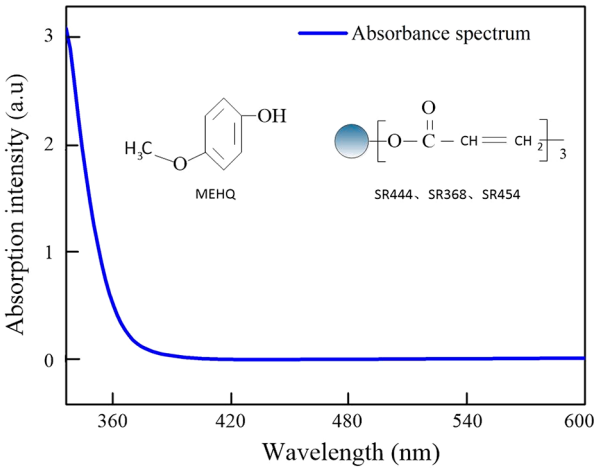

Figure 2. Single-photon absorbance spectrum of the developed PR. The monomers used in the photoresin are SR368, SR444, and SR454. These monomers are used to improve the chemical reactivity for high photosensitivity and mechanical strength and viscosity. MEHQ is an ultraviolet inhibitor.

Step 3: In Figure 3(c1), the groove of the HCF was filled with PR based on the capillarity effect. The PR used in this work was a negative resin. Then, the sample was mounted on a 3D air-bearing stage (Aerotech) for structure printing. The Fs laser has a central wavelength of 1026 nm, pulse width of 250 fs, and repetition rate of 220 kHz. To enhance the cohesive strength between the HCF and the printed structure, a pair of bases with the dimension of 800 μm × 6 μm × 10 μm was first printed along the inner surface of the HCF with a 50 × objective lens (NA = 0.7), the scanning speed of 4 mm/s and the laser intensity of 3.21 × 1012 W/cm^2. Then, the NF and Bragg grating segments are printed using a 63 × oil objective lens (NA = 1.4). To obtain an obvious Bragg resonance the same scanning speed of 200 μm/s but different laser intensities (3.82 × 10^{12} W/cm^2 for the NF and 5.82 × 10^{12} W/cm^2 for the grating segments) were chosen. An optical microscope image of the printed structure is shown in Figure 3 (c2).

Step 4: In Figure 3(d1), the sample was first immersed in a mixture of acetone and isopropyl alcohol (volume ratio: $^1/_3$) for 20 min to wash away the unpolymerized PR. Then it was placed in a drying oven (at 21%RH and 20 °C) to remove the residual moisture for 1 day.

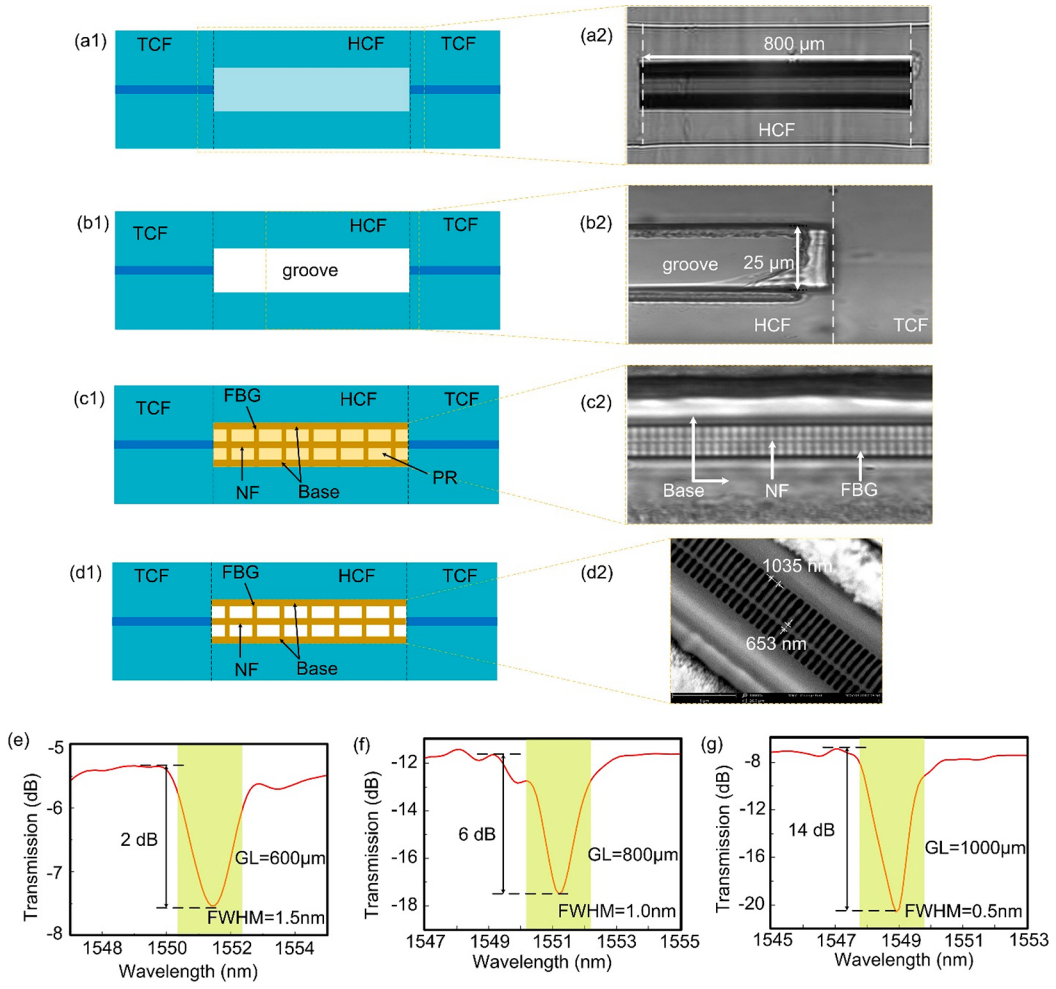

Figure 3. Schematic diagram of the polymer NFBG fabrication and the corresponding morphology of the dashed box. (a1) and (a2) An HCF was spliced between two TCFs. (b1) and (b2) A pair of rectangular grooves are drilled through the HCF by Fs laser. (c1) and (c2) The polymer NFBG was printed in the HCF. (d1) and (d2) The unpolymerized PR in the HCF was removed using an acetone and isopropyl alcohol mixture and the SEM image of the finished polymer structure containing a NF with a diameter of 653 nm and a Bragg grating with a pitch of 1035 nm. (e–g) Transmission spectra of three polymer NFBGs with different grating lengths (GL) of 600 μm, 800 μm, and 1000 μm.

DOI: 10.1021/acsami.9b16716
ACS Appl. Mater. Interfaces 2020, 12, 1465–1473

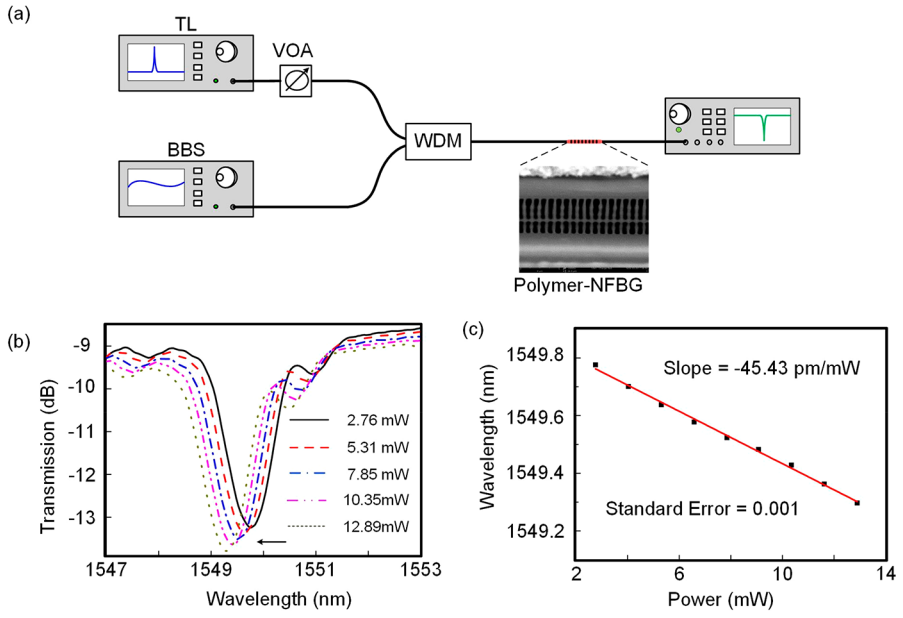

Figure 4. (a) Experimental setup of the static optical pump test. (b) Transmission spectral evolution of the probe light as the power of pump light increases from 2.7 mW to 12.9 mW. (c) The linear relationship between the Bragg resonant wavelength and pump power.

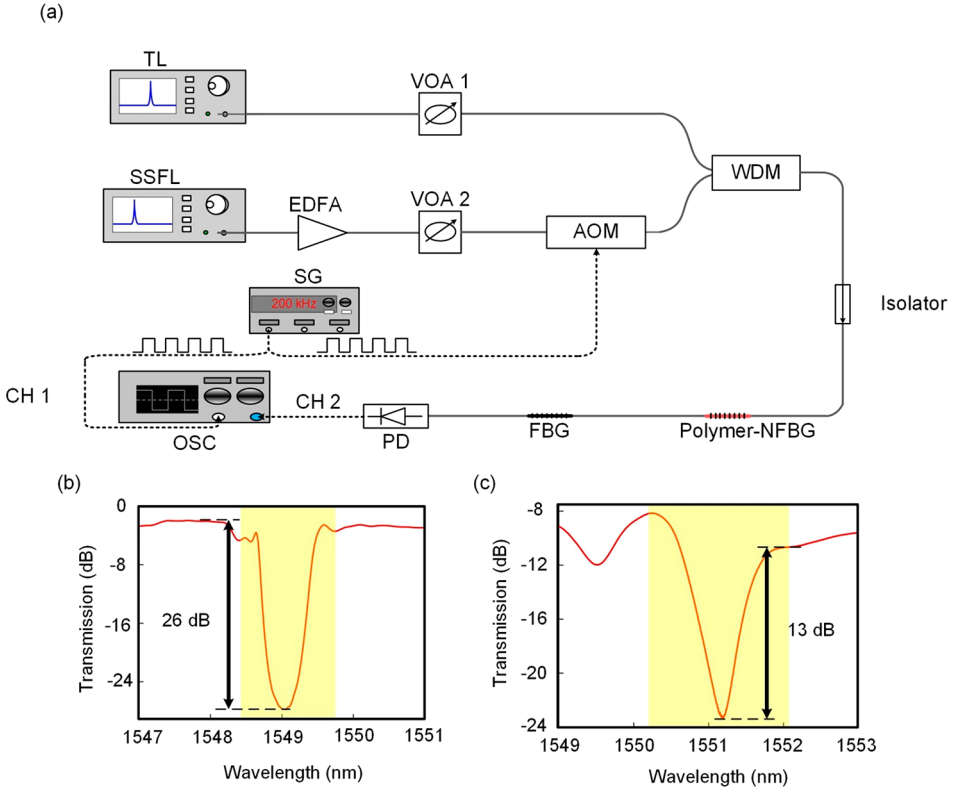

Figure 5. (a) Experimental setup of the dynamic optical pump test. (b) and (c) Transmission spectra of the homemade silica FBG and the polymer NFBG.

The NF diameter and the grating pitch were optimized as 653 and 1035 nm. Figure 3(d2) shows an SEM image of the top view of the finished polymer structure, where the printed structure is clear with no adhesion. Figure 3(e–g) compare the transmission spectra of three polymer NFBGs with different grating lengths (GL) of 1000 μm, 800 μm, and 600 μm (measured at 40% RH and 23 °C). In the spectra, an apparent Bragg resonance dip at ~1550 nm can be clearly observed. The relationship between Bragg resonant wavelength and the grating pitch can be described by

$$m\lambda_b = 2n_{\text{eff}}\Lambda \tag{9}$$

where m is the order of the Bragg resonance, λ_b is the resonant wavelength, n_{eff} is the mode effective refractive index, and Λ is the grating pitch. It is known that the resonance strength depends on the grating length and the modulation intensity.

DOI: 10.1021/acsami.9b16716
ACS Appl. Mater. Interfaces 2020, 12, 1465–1473

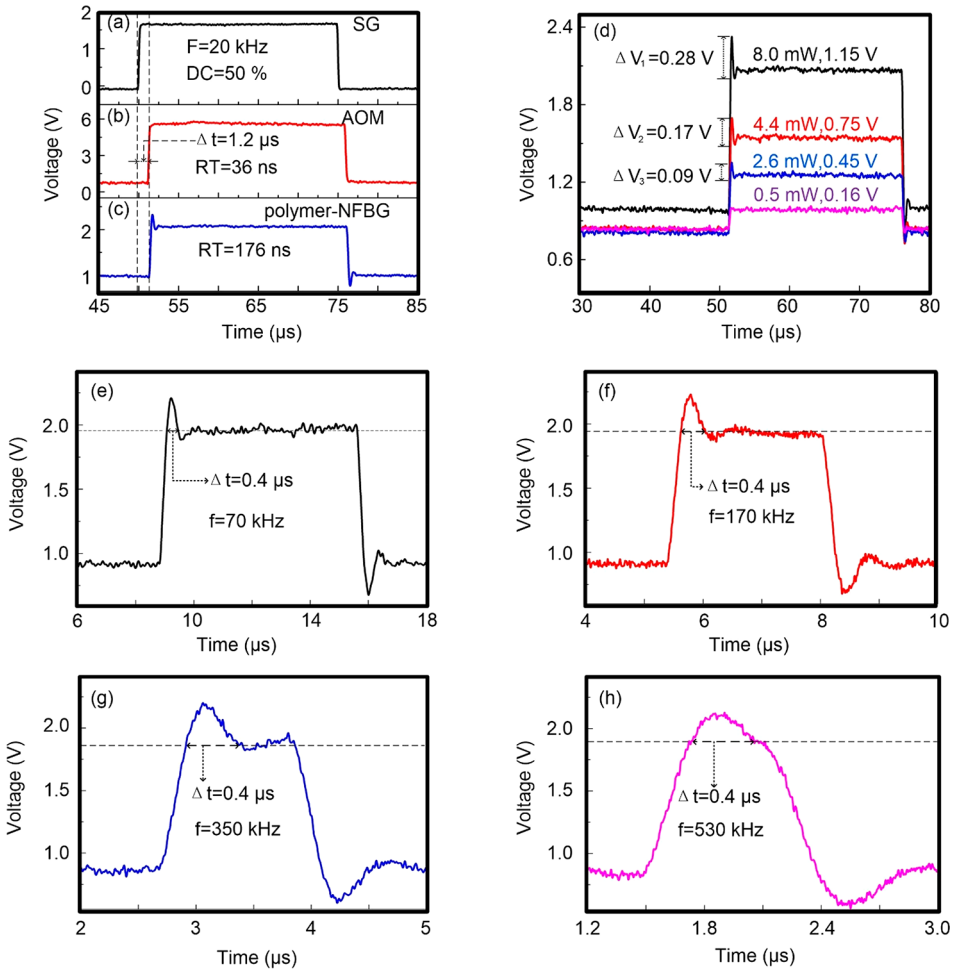

Figure 6. (a) The original signal from the signal generator (SG). Frequency (F) and duty cycle (DC). (b) The signal after the AOM. Time delay (Δt) and rising time (RT). (c) The signal after the polymer NFBG. (d) The output signal after the polymer NFBG with different pump powers. (e)−(h). Frequency response of the polymer NFBG with different pump frequencies: (e) 70 kHz, (f) 170 kHz, (g) 350 kHz, (h) 530 kHz.

With an increase of grating length from 600 to 1000 μm, the resonance strength increases from 2 to 14 dB, and the full width at half-maximum (fwhm) decreases from 1.5 to 0.5 nm, which is beneficial to improve the extinction ratio of the modulator. The insertion loss mainly results from the mode mismatch between the polymer NF and TCF.

4. TEST RESULT AND DISCUSSION

The experimental setup to study the static optical pump response is shown in Figure 4(a). The probe light from a broadband light source (BBS, 1250−1650 nm) and the pump light from a tunable laser (TL, Agilent 81638) were coupled into the polymer NFBG by use of a WDM coupler, and then the output signal was detected by an optical spectrum analyzer (OSA, Yokogawa AQ6370D). The wavelength of the pump light was tuned to the absorption band of the polymer at 1540 nm. The pump power of the pump light was adjusted by a variable optical attenuator (VOA). The transmission spectra of the polymer NFBG at different pump powers from 2.7 mW to 12.9 mW are shown in Figure 4(b), where a linear blueshift of the resonance dip was observed. The dip wavelengths at different pump powers are plotted in Figure 4(c), where the measured data are denoted by black squares and a linear fitting reveals the sensitivity of −45.43 pm/mW for the static pump response, and a pump power of 20 mW was estimated that it can induce the Bragg resonant wavelength shift of 0.5 nm with a modulation depth of 90%. The linear blueshift can be explained by the PT effect generated from light absorption of the polymer NF. When the pump beam, as a heat source, transits the polymer waveguide, the material would absorb partial light energy, and such energy would be released as thermal energy, which can lead the shift of the Bragg resonant wavelength.

The experimental setup to study the dynamic optical pump response is demonstrated in Figure 5(a).[33,34] The transmission spectrum of the polymer NFBG used is shown in Figure 5(c), where the resonant wavelength is 1551.2 nm and the dip strength is ∼13 dB. The probe light from a tunable laser (TL, Agilent 81638) was coupled into the polymer NFBG by a WDM coupler. To record the dynamic power variation of the probe light, its wavelength was tuned to the resonant wavelength of the polymer NFBG at 1551.2 nm and, provided the grating spectrum was shifted to short wavelength induced by the pump light, the probe light will be filtered along the rising edge of the grating spectrum, thereby causing an increase of optical power. Furthermore, the pump light from the single-frequency fiber laser (SFFL, Koheras, ADJUSTIK E15, 1549.0 nm) was first amplified by an erbium-doped fiber amplifier (EDFA) and then modulated by an acousto-optic modulator (AOM) with a periodic rectangular signal produced by a signal

DOI: 10.1021/acsami.9b16716
ACS Appl. Mater. Interfaces 2020, 12, 1465−1473

generator (SG). The driven signal was recorded in channel 1 of the oscilloscope (OSC, Tektronix MDO3054). The pump light was also coupled into the polymer NFBG to cause a periodic shift of the spectrum. In Figure 5(b), a homemade silica FBG with a dip strength of ~26 dB and a resonant wavelength of 1549.0 nm was used to block the pump light, and a fiber isolator was used to prevent the reflected light from returning to the tunable lasers. The output probe light was received by a photodetector (PD) and recorded in channel 2 of the OSC.

The original rectangular signal produced by the SG with a frequency of 20 kHz and a duty cycle (DC) of 50% is shown in Figure 6(a). The signal received after AOM is shown in Figure 6(b), where a rising time of 36 ns and a time delay of ~1.2 μs were observed and depended on the performance of the AOM. The signal received after the polymer NFBG is shown in Figure 6(c), where a rising time of 176 ns was observed, and two unexpected opposite photoacoustic (PA) signals were found at the end of the rising and falling courses in one cycle. The silica FBG almost filters the pump light. Thus, the signal from channel 2 after the polymer NFBG is the real time response of the device. Figure 6(d) compares the signals received after the polymer NFBG when the modulated-light power was set to 0.5 mW, 2.6 mW, 4.4 mW, and 8.0 mW, and the corresponding modulating amplitude and PA signal amplitude were measured as 0.16 and 0 V (at 0.5 mW); 0.45 and 0.09 V (at 2.6 mW); 0.75 and 0.17 V (at 4.4 mW); 1.15 and 0.28 V (at 8.0 mW), respectively. This device exhibits has higher temporal thermal response than other polymer devices.

The frequency response of the polymer NFBG was also investigated and the results at different input frequencies of 70 kHz, 170 kHz, 350 kHz, and 530 kHz are shown in Figure 6(e)−(h). As the input frequency increases, the output signal exhibits a serious distortion, but the PA-signal period remains unchanged being ~0.4 μs. Experimentally, when the pump light operates with a frequency of 1.44 MHz and a DC of 50%, the output signal was completely distorted and has only DC output. This means the frequency range of normal operation was under 1.44 MHz (see the Supporting Information).

The PA signal in the experiment may be explained by the interaction between the pump light and the polymer NF. The amplitude of PA signal only depends on the Grueneisen parameter of the material, which was mainly influenced by local temperature. Light absorption of the polymer NFBG releasing in the form of nonradiative heat will increase the local temperature and Grueneisen parameter. The PA signal was thus generated during the thermal confinement time in the polymer NFBG, and its amplitude was proportional to light irradiation $\varnothing(\mathrm{W/cm^2})$ within short rising period δt:[35,36]

$$p = \Gamma_0 \eta_{th} \mu_a \varnothing \delta t \tag{10}$$

where Γ_0 is the Grueneisen coefficient at ambient temperature, η_{th} is the heat conversion efficiency, and μ_a is the optical absorption coefficient.

In this work, two opposite PA signals generated at the end of the rising and falling courses can be explained by the change of Grueneisen coefficient when the polymer NFBG was heated by the pump light. As shown in Figure 6(d), when the modulated-light power was 0.5 mW, the PA signal was difficult to detect for low deformation and with an increase of pump power, the amplitude of the PA signal increases gradually. If the duration of the heat equilibration was shorter than the modulation period, the PA signal kinetics can be extracted from the diffusive part of the signal, as shown in Figure 6(e)−(g). If the heat equilibration cannot be completed within one modulation period, the PA signal kinetics cannot be determined from the rising edge of the signal, as shown in Figure 6(h).

The photoannealing phenomenon has been found for the polymer NFBG. Experimentally, when the power of the pump light was over 50 mW, the resonance dip will first experience a fast blueshift and then a slight redshift and finally stabilize permanently. This phenomenon is referred to as the photoannealing effect and can be explained by the fact that with the long-term irradiation of high power light, the molecules cluster, and the polymer molecular chain breaks and then further polymerizes with the free polymer monomers.[37] If the light power continues to increase, the redshift will become more obvious. Figure 7(a) and (b) compares the transmission spectra of the polymer NFBG before and after photoannealing. The resonant wavelength shifted from 1551.2 to 1553.1 nm, the extinction ratio decreased from 6 to 0.7 dB, and the insertion loss (@1560 nm) decreased from 11.5 to 5.1 dB. The resonant wavelength and the extinction ratio cannot be recovered. This means the light power threshold of normal operation is 50 mW.

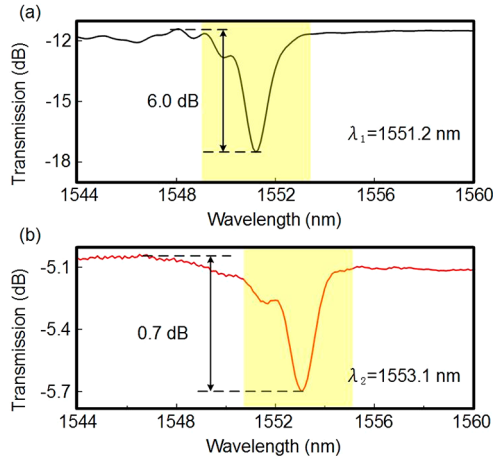

Figure 7. (a) Initial transmission spectrum of the polymer-NFBG. (b) Transmission spectrum of the polymer-NFBG after photoannealing treatment.

As a polymer device, the humidity influence should be noticed. The humidity response of the polymer NFBG was studied by controlled humidity chambers.[38] The humidity measurement was carried out at 25 °C, and the Bragg resonant wavelength was used to monitor the humidity change. The chamber was programmed to increase the humidity from 30% RH to 90% RH with a step of 20% RH. Fifteen min was used to increase the humidity, followed by another 15 min for stabilization. The transmission spectral evolution is demonstrated in Figure 8, where the Bragg resonance exhibits a significant blueshift and the dip strength decreases as the humidity rises. This means the humidity range of normal operation was from 30% RH to 50% RH, which can be guaranteed by use of suitable package.[39]

5. CONCLUSIONS

A new type of high-speed fiber-integrated all-optical modulator based on a polymer NFBG has been demonstrated. Such an optical modulator exhibits a high pump sensitivity of −45.43

DOI: 10.1021/acsami.9b16716
ACS Appl. Mater. Interfaces 2020, 12, 1465−1473

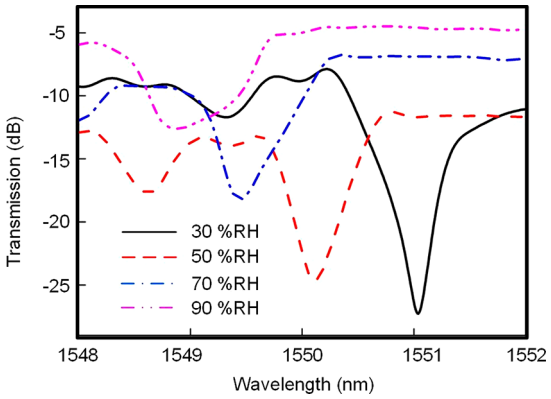

Figure 8. Transmission spectral evolution of the polymer NFBG as the humidity increases from 30% RH to 90% RH.

pm/mW and a fast temporal response of 176 ns and excellent linear response. The PA signals (~0.4 μs), which occur at the end of the rising and falling courses in each cycle, are produced by the light absorption in the polymer NFBG. The PA signal may find potential application in sensors. Moreover, the light power threshold of normal operation was 50 mW and the optimized working humidity wa from 30% RH to 50% RH. This work provides a brand-new method to develop fiber-integrated polymer devices.

■ ASSOCIATED CONTENT

Supporting Information

The Supporting Information is available free of charge at https://pubs.acs.org/doi/10.1021/acsami.9b16716.

Video aims to prove that the frequency response of the device demonstrated by us can reach 1.44 MHz. From the video, the original rectangular signal (yellow line) produced by the signal generator displays in the screen and the detected signal from the all-optical modulator is the blue line. With the frequency of original signal increasing, the detected signal intends to be distorted, and when the frequency reaches 1.44 MHz, the blue line becomes a straight line. Therefore, it proves that this device can respond to signals below 1.44 MHz. However, due to the defects of the signal generator, when the original signal frequency increases above 1.0 MHz, there is a distortion at the rising edge of the rectangular wave (yellow line) (MP4)

■ AUTHOR INFORMATION

Corresponding Author

*E-mail: cliao@szu.edu.cn.

ORCID

Changrui Liao: 0000-0003-0233-8403

Ying Wang: 0000-0001-8020-3622

Author Contributions

⊥These authors contributed equally to this work.

Notes

The authors declare no competing financial interest.

■ ACKNOWLEDGMENTS

C. R. L. and C. L. have the same contribution to this paper. C. R. L. and C. L. conceived the experiment. C. L. made the devices, built the experimental setup, and carried out the experiments. C. L. and C. R. L. wrote the manuscript. C. L., C. R. L., Y. P. W., Y. W., J. H., and S. L. analyzed the data. Z. S. G. synthesised the photoresist. All authors have given approval to the final version of the manuscript. Thanks to The National Natural Science Foundation of China (NSFC) (61575128, 61425007), The Natural Science Foundation of Guangdong Province (2018B030306003), The Science and Technology Innovation Commission of Shenzhen (KQJSCX20170727101953680, JCYJ20180507184503128, JCYJ20170818100431895), and Development and Reform Commission of Shenzhen Municipality Foundation.

■ REFERENCES

(1) Xu, Q. F.; Schmidt, B.; Pradhan, S.; Lipson, M. Low-loss Plasmon-assisted Electro-optic Modulator. *Nature* **2005**, *435*, 325−327.

(2) Xie, J. Y.; Hu, X. Y.; Li, C.; Wang, F. F.; Xu, P. Z.; Tong, L. M.; Yang, H.; Gong, Q. H. On-Chip Dual Electro-Optic and Optoelectric Modulation Based on ZnO Nanowire-Coated Photonic Crystal Nanocavity. *Adv. Opt. Mater.* **2018**, *6*, 1800374.

(3) Mukherjee, S.; Maiti, R.; Midya, A.; Das, S. Tunable Direct Bandgap Optical Transitions in MoS 2 Nanocrystals for Photonic Devices. *ACS Photonics* **2015**, *2*, 760−768.

(4) Hisakado, Y.; Kikuchi, H.; Nagamura, T.; Kajiyama, T. Large Electro-optic Kerr Effect in Plymer-Stabilized Liquid-Crystalline Blue Phases. *Adv. Mater.* **2005**, *17*, 96−98.

(5) Chembo, Y. K.; Strekalov, D. V.; Yu, N. Spectrum and Dynamics of Optical Frequency Combs Generated with Monolithic Whispering Gallery Mode Resonators. *Phys. Rev. Lett.*, **2010**, DOI: 10.1103/PhysRevLett.104.103902.

(6) Yu, S. L.; Wu, X. Q.; Chen, K.; Chen, B. G.; Guo, X.; Dai, D. X.; Tong, L. M.; Liu, W. T.; Shen, Y. R. All-optical Graphene Modulator Based on Optical Kerr Phase Shift. *Optica* **2016**, *3*, 541−544.

(7) Mao, D.; Cui, X. Q.; Gan, X. T.; Li, M. K.; Zhang, W. D.; Lu, H.; Zhao, J. L. Passively Q-Switched and Mode-Locked Fiber Laser Based on an ReS 2 Saturable Absorber. *IEEE J. Sel. Top. Quantum Electron.* **2018**, *24*, 1100406.

(8) Szukalski, A.; Moffa, M.; Camposeo, A.; Pisignano, D.; Mysliwiec, J. All-optical Switching in Dye-doped DNA Nanofibers. *J. Mater. Chem. C* **2019**, *7*, 170−176.

(9) Grobnic, D.; Mihailov, S. J.; Ballato, J.; Dragic, P. D. Type I and II Bragg gratings made with Infrared Femtosecond Radiation in High and Low Alumina Content Aluminosilicate Optical Fibers. *Optica* **2015**, *2*, 313−322.

(10) Grobnic, D.; Smelser, C. W.; Mihailov, S. J.; Walker, R. B. Long-term Thermal Stability Tests at1000° C of Silica fiber-FiberBragg Gratings Made with Ultrafast Laser Radiation. *Meas. Sci. Technol.* **2006**, *17*, 1009−1013.

(11) Liao, C. R.; Wang, D. N.; Li, Y. H.; Sun, T. V.; Grattan, K. T. Temporal Thermal Response of Type II−IR Fiber Bragg Gratings. *Appl. Opt.* **2009**, *48*, 3001−3007.

(12) Li, Y. L.; Fang, Y. F.; Wang, J.; Wang, L.; Tang, S. W. Integrative Optofluidic Microcavity with Tubular Channels and Coupled Waveguides via Two-Photonpolymerization. *Lab Chip* **2016**, *16*, 4406−4414.

(13) Kawata, S.; sun, H.-B.; Tanaka, T.; Takada, K. Finer Features for Functional Microdevices - Micromachines can be Created with Higher Resolution using Two-Photon Absorption. *Nature* **2001**, *412*, 697−698.

(14) Gissibl, T.; Thiele, S.; Herkommer, A.; Giessen, H. Two-Photon Direct Laser Writing of Ultracompact Multi-lens Objectives. *Nat. Photonics* **2016**, *10*, 554−560.

(15) Markos, C.; Stefani, A.; Nielsen, K.; Rasmussen, H. K.; Yuan, W.; Bang, O. High-Tg TOPAS Microstructured Polymer Optical Fiber for Fiber Bragg Grating Strain Sensing at 110 Degrees. *Opt. Express* **2013**, *21*, 4758−476.

(16) Woyessa, G.; Fasano, A.; Markos, C.; Rasmussen, H.; Bang, O. Low loss Polycarbonate Polymer Optical Fiber for High Temperature FBG Humidity Sensing. *IEEE Photonics Technol. Lett.* **2017**, *29*, 57.
(17) Balčytis, A.; Ryu, M.; Juodkazis, S.; Morikawa, J. Micro-thermocouple on Nano-membrane: Thermometer for Nanoscale Measurements. *Sci. Rep.* **2018**, *8*, 6324.
(18) Wang, P.; Wang, Y. P.; Tong, L. M. Functionalized Polymer Nanofibers: AVersatile Platform for Manipulating Light at the Nanoscale. *Light: Sci. Appl.* **2013**, *2*, No. e102.
(19) Hida, Y.; Onose, H.; Imamura, S. Polymer Waveguide Thermooptic Switch with Low Electric Power Consumption at 1.3 μm. *IEEE Photonics Technol. Lett.* **1993**, *5*, 1041−1135.
(20) Nikolajsen, T.; Leosson, K. Surface Plasmon Polariton Based Modulators and Switches Operating at Telecom Wavelengths. *Appl. Phys. Lett.* **2004**, *85*, 5833−5835.
(21) Liu, H. L.; Shi, Y.; Liang, L.; Li, L.; Guo, S. S.; Yin, L.; Yang, Y. A Liquid Thermal Gradient Refractive Index Lens and Using it to Trap Single Living Cell in Flowing Environments. *Lab Chip* **2017**, *17*, 1280−1286.
(22) Liang, L.; Zhu, X. Q.; Liu, H. L.; Shi, Y.; Yang, Y. A Switchable 3D Liquid−liquid Biconvex Lens with Enhanced Resolution Using Dean Flow. *Lab Chip* **2017**, *17*, 3258.
(23) Jin, W.; Cao, Y. C.; Yang, F.; Ho, H. L. Ultra-sensitive All-fiberPhotothermal Spectroscopy with Large Dynamic Range. *Nat. Commun.* **2015**, *6*, 6767.
(24) Digonnet, F. M. J.; Kim, H. K.; Kino, G. S.; Fan, S. Understanding Air-core Photonic-bandgap Fibers: Analogy to Conventional Fibers. *J. Lightwave Technol.* **2005**, *23*, 4169−4177.
(25) Bialkowski, S. E. *Photothermal Spectroscopy Methods for Chemical Analysis*; John Wiley & Sons, 1996.
(26) Morris, M. D.; Peck, K. Photothermal Effects in Chemical Analysis. *Anal. Chem.* **1986**, *58*, 811−822.
(27) Goyanes, S. N.; Marconi, J. D.; Rubiolo, G. H. Analysis of Thermal Diffusivity in Aluminum (particle)-filled PMMA Compounds. *Polymer* **2001**, *42*, 5267−5274.
(28) Weidenfeller, B.; Hofer, M.; Schiling, F. R. Thermal conductivity, Thermal Diffusivity, and Specific heat Capacity of Particle Filled Polypropylene. *Composites, Part A* **2004**, *35*, 423−429.
(29) Gensch, T.; Viappiani, C. Time-resolved Photothermal Methods: Accessing Time-resolved Thermodynamics of Photo-induced Processes in Chemistry and Biology. *Photochem. Photobiol. Sci.* **2003**, *2*, 699−721.
(30) Mihailov, S. J.; Smelser, C. W.; Lu, P.; Walker, R. B.; Grobnic, D. Fiber Bragg Gratings made with a Phase Mask and 800-nm Femtosecond Radiation. *Opt. Lett.* **2003**, *28*, 995−997.
(31) Li, C.; Liao, C. R.; Wang, J.; Gan, Z. S.; Wang, Y. P. Femtosecond Laser Microprinting of a Polymer Optical Fiber Interferometer for High-Sensitivity Temperature Measurement. *Polymers* **2018**, *10*, 1192.
(32) Li, C.; Liao, C. R.; Wang, J.; Li, Z. Y.; Wang, Y.; He, J.; Bai, Z. Y.; Wang, Y. P. Femtosecond Laser Microprinting of a Polymer Fiber Bragg Grating for High-sensitivity Temperature Measurements. *Opt. Lett.* **2018**, *43*, 3409−3412.
(33) Majumder, M.; Gangopadhyay, T. K.; Chakraborty, A. K.; Dasgupta, K.; Bhattacharya, D. K. Fiber Bragg Gratings in Structural Health Monitoring—Present Status and Applications. *Sens. Actuators, A* **2008**, *147*, 150−164.
(34) Schmidt, C.; Chipouline, A.; Pertsh, T.; Tunnermann, A.; Egorov, O. Nonlinear Thermal Effects in Optical Microspheres at Different Wavelength Sweeping Speeds. *Opt. Express* **2008**, *16*, 6285−6301.
(35) Lai, P.; Wang, L.; Tay, J. W.; Wang, L. V. Photoacoustically Guided Wavefront Shaping for Enhanced Optical Focusing in Scattering Media. *Nat. Photonics* **2015**, *9*, 126−132.
(36) Wang, L.; Zhang, C.; Wang, L. V. Grueneisen Relaxation Photoacoustic Microscopy. *Phys. Rev. Lett.* **2014**, *113*, 174301.
(37) Woyessa, G.; Pedersen, J. K. M.; Fasano, A.; Nielsen, K.; Bang, O. Zeonex-PMMA Microstructured Polymer Optical FBGs for Simultaneous Humidity and Temperature Sensing. *Opt. Lett.* **2017**, *42*, 1161−1164.
(38) Chen, R.; Wang, X.; Yao, X. K.; Zheng, X. C.; Wang, J.; Jiang, X. Q. Near-IR-triggered Photothermal/photodynamic Dual-modality Therapy System via Chitosan Hybrid Nanospheres. *Biomaterials* **2013**, *34*, 8314−8322.
(39) Li, Z. Y.; Liao, C. R.; Song, J.; Wang, Y.; Zhu, F.; Wang, Y. P.; Dong, X. P. Ultrasensitive Magnetic Field Sensor Based on an In-Fiber Mach−Zehnder Interferometer with a Magnetic Fluid Component. *Photonics Res.* **2016**, *4*, 197−201.

DOI: 10.1021/acsami.9b16716
ACS Appl. Mater. Interfaces 2020, 12, 1465−1473